http://www.glaciology.ethz.ch

CLIMATE WARMING AND STABILITY OF COLD HANGING GLACIERS: LESSONS FROM THE GIGANTIC 1895 ALTELS BREAK-OFF

J. FAILLETTAZ, D. SORNETTE, AND M. FUNK

Abstract. The Altels hanging glacier broke off on September 11, 1895. The ice volume of this catastrophic rupture was estimated at 4.10^6 cubic meters and is the largest ever observed ice fall event in the Alps. The causes of this collapse are however not entirely clear. Based on previous studies, we reanalyzed this break-off event, with the help of a new numerical model. This model, initially developed by Faillettaz and others (2010) for gravity-driven instabilities, was applied to this glacier. The model takes into account the progressive maturation of a heterogeneous mass towards a gravity-driven instability, characterized by the competition between frictional sliding and tension cracking. We use an array of sliding blocks on an inclined (and curved) basal surface, which interact via elastic-brittle springs. A realistic state- and rate-dependent friction law is used for the block-bed interaction. We model the evolution of the inner material properties of the ice and its progressive damage eventually leading to failure, by means of a stress corrosion law governing the rupture of the springs. The simulations indicate that a break-off event is only possible when the basal friction at the bedrock is reduced in a restricted area, possibly induced by the storage of infiltrated water within the glacier. This result is in agreement with the fact that the collapse occurred after several hot summers. Moreover, our simulations reveal a two-step behavior: (i) A first quiescent phase, without visible changes, with a duration depending on the rate of basal changes; (ii) An active phase with a rapid increase of basal motion over a few days. As a consequence, a crown crevasse is predicted to open within a few days (which was observed) prior to the occurrence of the final collapse. The general lesson obtained from the comparison between the simulations and the available evidence is that visible signs of the destabilization process of a hanging glacier, resulting from a progressive warming of the ice/bed interface towards a temperate regime, will appear just a few days prior to the collapse.

1. Introduction

Icefalls pose a considerable risk to humans, settlements and infrastructures. The destructive power of this natural phenomenon is usually greater in winter as it may drag snow and ice on its train. In the Alps, one of the most tragic ice fall event occurred in 1965 in Switzerland, when a major part of Allalin glacier broke off and killed 88 employees of the Mattmark dam construction site (Röthlisberger, 1981; Raymond and others, 2003). Following this event, interest in the instability of hanging glacier grew within the alpine glaciological community. In 1973, the first successfull icefall prediction was performed by Flotron (1977) and Röthlisberger (1981) at the Weisshorn glacier, which pose regulary a threat to the village of Randa (Valais, Switzerland). Due to climatic variations, some hanging glaciers

Key words and phrases. glacier, rupture, modelling, climate warming.

undergo rapid changes leading either to isolated catastrophic events, or to new situations with no historical precedent. Direct measurements are difficult to perform on these steep, heavily crevassed and avalanche-endangered glaciers. These measurements are often sparse and fragmentary, and therefore difficult to interpret. They were always performed after clear signs of destabilization. The conditions prevailing before an unstable state are thus unknown. The factors responsible for the destabilization of large ice masses are the strength of the ice and the stresses in the zone of fracture. However, the physics of the ice fracture and the feedback mechanisms between crevassing, ice deformation and load distribution are complex and mostly unknown. Lack of theory and sparse measurements make an accurate stability assessment difficult.

To cope with these difficulties, we developed a numerical model describing the progressive maturation of a mass towards a gravity-driven instability, which combines basal sliding and cracking (described in Faillettaz and others (2010)). Our primary hypothesis was that gravity-driven ruptures in natural heterogeneous material are characterized by a common triggering mechanism resulting from a competition between frictional sliding and tension cracking.

The present paper is devoted to the application of this general numerical model to a particular gravity-driven instability: the breaking-off of hanging glaciers. The gigantic breaking-off of the Altels hanging glacier is an interesting case for several reasons: (i) This break-off is the largest ever observed and recorded in the Alps. (ii) This catastrophic phenomenon was very well documented as Heim (1895), Forel (1895) and Du Pasquier (1896) described, within the limit of their knowledge, their observations related to the rupture of the glacier and made some photographs of the glacier before and after the collapse. (iii) The causes of this glacier instability are not entirely understood, despite the reanalysis made by Röthlisberger (1981) of the data collected by Heim (1895), Forel (1895), Du Pasquier (1896). However, hot summers prior to the event are suspected to have triggered this break-off. (iv) This is the only well documented break-off of a cold hanging glacier, where a progressive warming of the ice-bed interface towards temperate conditions likely has driven the phenomenon. (iv) Furthermore, the study of this break-off is of interest in the context of global climate warming. This study should help to better understand the processes leading to this catastrophic phenomenon. Moreover, it should give new insights on the probable causes of this particular gravity-driven instability and reveal precursors of this event.

Section 2 describes the study site and the qualitative description of the rupture. Section 3 describes how the model is implemented and section 4 presents the main qualitative and quantitative results.

2. Study site: Altels

2.1. **Generality and description of the catastrophe.** The Altels (Berner Oberland, Switzerland) is 3629 m above see-level and has a pyramidal shape. The northwestern flank is 1500 m high and 35° to 40° steep (Fig. 1). It consists of relatively smooth malm limestone (Fig. 4). In the middle of the 19th century, this face was largely covered with an unbalanced ramp glacier (Pralong and Funk, 2006) located between 3629 m and 3000 m above sea level.

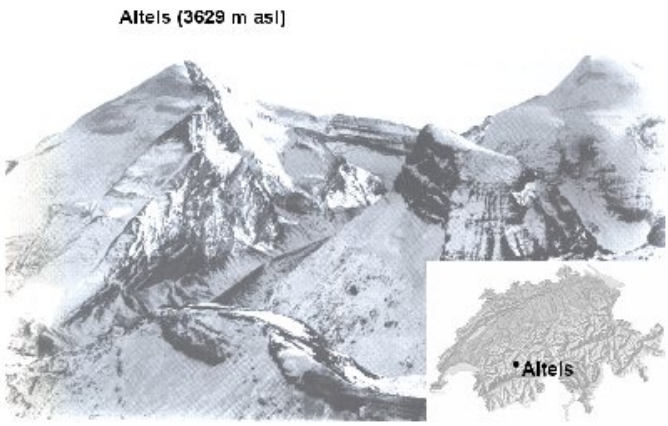

FIGURE 1. Overview of the Altelsgletscher in November 25 1894, ten months before the glacier break-off. Photo P. Montandon from Englistliggrat, 2665 m asl

In the early morning of September 11, 1895, a large part of this glacier broke off and tumbled down. This ice fall lasted about one minute and the accompanying thunder could be perceived in Kandersteg (about 10 km away). Many people thought it was an earthquake. This catastrophic break-off was carefully described and reported by Heim (1895), Forel (1895), Du Pasquier (1896) and later on by Röthlisberger (1981).

The volume of the break-off was estimated at 4 Millions cubic meters, which is the largest known glacial fall in the Alps. The resulting ice avalanche ravaged the high mountain pasture situated underneath called the Spittelmatte and caused the death of 6 persons and 170 cows. Four huts and large forest parts were also destroyed and great quantities of cheese ruined (which was an economic disasters for the bereaved families). Due to its huge velocity (i.e. 430 km/h Heim, 1895; Röthlisberger, 1981), this avalanche pilled 300 m up on the opposite slope towards the Üschinengrat (Fig. 3). An area of about one square km of the pasture was buried under a 3 to 5 meters thick ice layer. As Forel (1895) reported, a similar event had already occurred at the same place in 1782, killing 4 persons and hundreds of domestic animals (Raymond and others, 2003). Forel (1895) pointed out that, at that time, the summer was warmer than usual. Nowadays, this won't happen any more because the Altels glacier has almost disappearred (a tongue remains on its left side, which will melt away in the near future, Fig. 4).

2.2. **Rupture and probable causes.** The shape of the crown crack was a huge regular parabolic-like arch with a width of about 580 meters (Figs. 2 and 4). The ice thickness at the crown crack was around 40 meters and 20 meters at the basis (Fig. 4). The finale rupture took place and propagated along the bedrock.

Forel (1895) analysed the causes of the rupture mechanism. He pointed out the extremely hot previous summers as a possible link to this catastrophe. This argument could explain why the glacier was no longer mostly frozen within the bedrock and lost adhesion due to a thin film of water between the bedrock and the

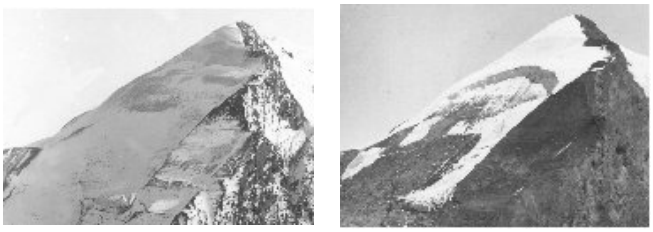

FIGURE 2. Altels glacier before and after its break-off (Photo P. Montandon, 25 November 1894 and 15 September 1895; Archiv des Alpinen Museums Bern)

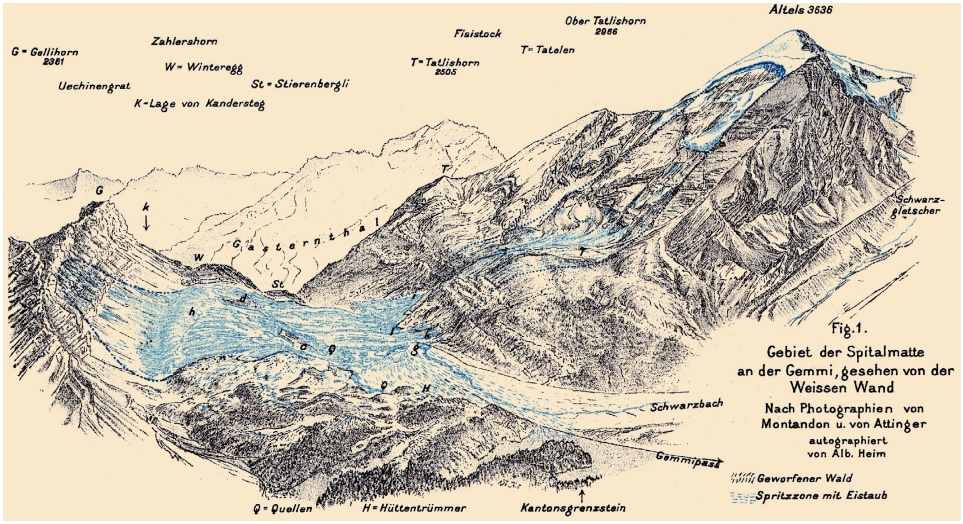

FIGURE 3. General overview of the catastrophe (after Heim 1895).

FIGURE 4. Link: Side glacier remaining in 1979. Bedrock consists of malm limestone. Photo from H. Röthlisberger. Right: Altels nowadays.

ice. Röthlisberger (1981) reanalyzed the documented field observations from Heim (1895); Forel (1895); Du Pasquier (1896) to infer the thermal conditions of Altels glacier before its break-off (Fig. 5). He argued, from Fig. 2 that:

(i) Above the bergschrund, the glacier was frozen onto its bedrock and ice temperature should be below melting point.

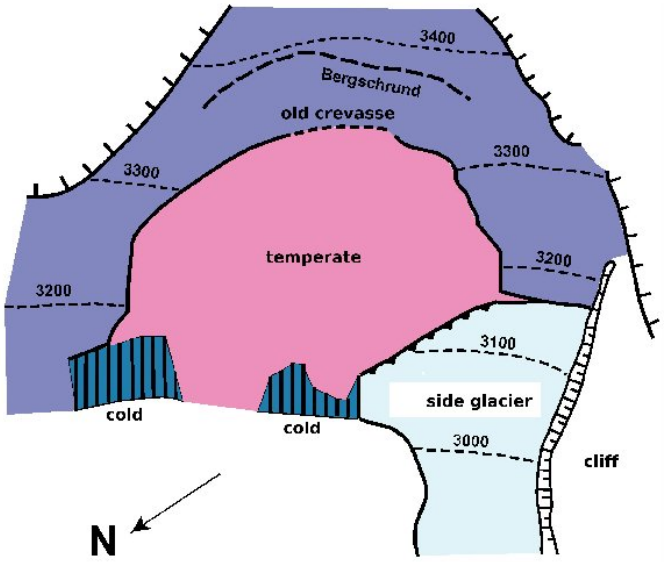

FIGURE 5. Schema of the supposed thermal conditions at the bedrock and in the glacier before its break-off (after Röthlisberger, 1981).

(ii) Below the bergschrund, ice and firn were temperate: it is possible to distinguish on Fig. 2 a flat area covered by snow. By melting, this snow may have warmed up the ice and eventually melted water could have percolated through the glacier down to the bedrock.

(iii) Further down, the snow cover lying on the glacier was very thin because of the strong wind erosion. Röthlisberger (1981) argued that ice was likely be cold in this area, as the thermic isolation from the snow cover is less effective in colder season (Fig. 2). Moreover, he argued that melted water had no time to percolate and warm the glacier, as the slope is very large in this area.

(iv) The glacier was frozen to the bedrock at the margins and temperate in the middle (Figs. 2 and 4). At the margins, some remaining ice can be recognized (white spots), indicating that the glacier was still frozen on the bedrock.

Röthlisberger (1981) analysed the retaining forces of the hanging glacier and the possible causes of the break-off.

(i) Adhesion to the bedrock: Given the dimensions of the unstable ice slab compared to its thickness, the basal properties should play a crucial role on the global stability. The existence of temperate conditions at the interface between bedrock and the glacier is a destabilizing process that favours sliding of the glacier on its bed. When the glacier slides over bumps or bedrock asperities, cavities forms above the bedrock leading to a lost of adhesion of the glacier on the bedrock. Moreover, melting and high water pressure at the interface favour and accelerate the enlargement of the cavities. This could lead to a destabilization of the glacier in a very short time (from 1

day to 1 week). Precursors of such destabilization process would be hardly detectable as such cavities can not be easily evidenced from the surface.

(ii) Southern support of the side glacier: The side glacier could also play an important role on the global stability of the hanging glacier. From Fig. 1, it is possible to distinguish an opened crevasse on the side glacier prolongated into the Altels glacier ten months before the rupture. This could have formed because of sliding of the side glacier, which acts as a support for the whole glacier. Such a sliding phenomenon was already observed in 1895 and a sliding of 25/30 m/year was also observed in 1927/28 (Röthlisberger, 1981).

(iii) Support of the frozen margins: It is possible that the lateral support of the frozen margins had a considerable role on the stability of the glacier, especially because of the important surface melting of the glacier two years before the rupture (from photo in Du Pasquier, 1896). Du Pasquier (1896) and Heim (1895) analysed temperature data from different locations in Switzerland and found that the summer 1895 was exceptionnaly warm. With the prevailing climate conditions, sufficient melted water could have been produced to weaken the basal frozen support.

(iv) Traction at the crown crack (cohesion): As the shape of the crown crack is a nearly perfect arch, it seems that before the destabilization phase, the glacier was in a mechanical equilibrium. The crown crack was already slightly opened with a limited depth ten month before the rupture (see Fig. 2), indicating large tensile stresses.

2.3. **Temperature and precipitation before 1895.** As Heim (1895); Forel (1895) and Röthlisberger (1981) pointed out that very warm summers (i.e. generating much more melted water than earlier) are suspected to have favoured the instability, we investigated the evolution of the climatic conditions at the Altelsgletscher before its 1895 break-off. A data base with homogenized continuous daily time series of temperature and precipitation since 1865 are available at the Federal Office of Meteorology and Climatology MeteoSwiss. The time series are corrected for systematic biases which may be due, for example, to the relocation of the weather station or changing measuring techniques (Begert and others, 2005). A total of 12 MeteoSchweiz stations are available but we used the two closest stations, one located in Sion (35 km away) and other in Bern (60 km away).

Air temperature is known to be relatively well correlated over large distances (Begert and others, 2005) and can therefore be extrapolated with confidence. We evaluated the temperature at 3000 m a.s.l. by applying a temperature gradient of -6°C per 1000m on the mean daily values from the two meteo stations. The extrapolation of solid precipitations are more problematic. As a first approximation, we computed the mean precipitations from the two stations and considered it to be solid when the extrapolated temperature at 3000 m was below 0°C.

Daily snow and ice melt rates can be assumed proportional to the positive degree day (Hock, 2003). Because the albedo of ice is lower than for snow, the melting will be larger when the annual snow cover has disappeared. The rate of solid precipitation and the sum of the Positive Degree Days (PDD) is an indication on the annual mass balance of the glacier, i.e. a small annual solid precipitation rates would lead to an earlier disappearance of the snow cover and therefore to higher melt rates because of a longer time with low albedo.

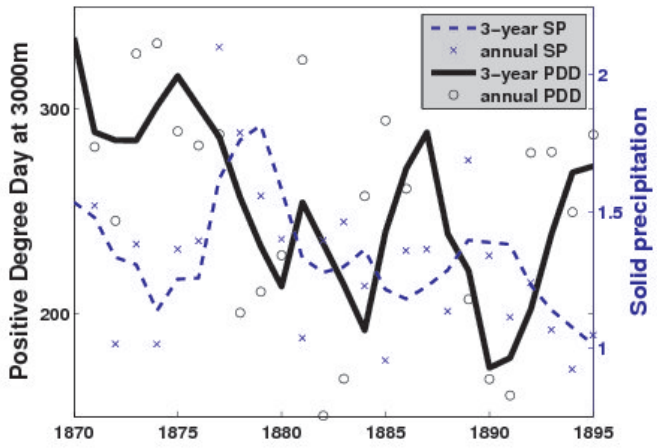

FIGURE 6. 3-year running mean of Positive Degree Days (solid black line) and solid precipitation (dashed line) between 1870 and 1895 at 3000 m a.s.l. at the location of the 1895 Altels break-off. Annual values are also indicated (circles for PDD and crosses for solid precipitations).

Time series of Positive Degree Days (PDD) since 1870 (Fig. 6) indicated larger value in the 1870's and an increasing trend 5 years before 1895. Moreover, solid precipitation has decreased during this period indicating less winter accumulation. Five years before the break-off, the glacier experienced smaller annual mass balances (decrease of solid precipitation combined with a larger PDD). These results are compatible with the descriptions of Heim (1895) and Röthlisberger (1981).

3. Numerical modelling

The aim of the present work is to reanalyse this event by applying a new numerical model designed for describing natural gravity-driven instabilities (Faillettaz and others, 2010). This model allows us to test the different hypotheses previously published to explain the break-off of this glacier.

3.1. **Model description.** We use a model describing the progressive maturation of a mass towards a gravity-driven instability, which combines basal sliding and cracking. Our hypothesis is that gravity-driven ruptures in natural heterogeneous materials are characterized by a common triggering mechanism resulting from a competition between frictional sliding and tension cracking. Heterogeneity of material properties and dynamical interaction seem to have a significant influence on the global behavior.

This numerical model is based on the discretization of the natural medium in terms of blocks and springs forming a two-dimensional network sliding on an inclined plane. Each block, which can slide, is connected to its four neighbors by springs that can fail, depending on the history of displacements and damage. We develop physically realistic models describing the frictional sliding of the blocks on

the supporting surface and the tensile failure of the springs between blocks proxying for crack opening. Frictional sliding is modeled with a state-and-velocity weakening friction law with threshold. Crack formation is modeled with a time-dependent cumulative damage law with thermal activation including stress corrosion. In order to reproduce cracking and dynamical effects, all equations of motion (including inertia) for each block are solved simultaneously.

The run-up to the sliding instabilities can be described by applying a modern constitutive law of state-and-velocity dependent friction. This means that solid friction is not used as a parameter but as a process evolving with the concentration of deformation and properties of sliding interfaces. Cracking and fragmentation in the mass is accounted for by using realistic laws for the progressive damage accumulation via stress corrosion and other thermally activated processes aided by stress.

The present model improves the multi-block model of Andersen and others (1997) and Leung and Andersen (1997) in two ways. First, we use a state-and-velocity weakening friction law instead of a constant (or just state- or velocity-weakening) solid friction coefficient. Second, rather than a static threshold for the spring failures, we model the progressive damage accumulation via stress corrosion and other thermally activated processes aided by stress. Both improvements make the numerical simulations significantly longer but present the advantage of embodying rather well the known empirical phenomenology of sliding and damage processes. Adding the state and velocity-dependent friction law and time-dependent damage processes allows us to model rather faithfully the interplay between sliding, cracking between blocks and the overall self-organizing of the system of blocks.

The geometry of the system of blocks interacting via springs and with a basal surface is depicted in Figure 7. To sum up, the model includes the following characteristics:

(1) Frictional sliding on the ground or between layers,
(2) Heterogeneity of basal properties,
(3) Possible tension rupture by accumulation of damage,
(4) Dynamical interactions of damage or cracks along the sliding layer,
(5) Geometry and boundary conditions, and
(6) Interplay between frictional sliding and cracking.

The different steps describing how development of the instability is modelled are plotted in Figure 8. As explained previously, two phases have to be distinguished:

(i) A quasi-static (quiescent) phase corresponding to the nucleation of block sliding and bond rupture.
(ii) A dynamical (active) phase corresponding to the sliding phase of the blocks and of the failure of bonds.

To account for the changes of the surface characteristics after blocks have slid, a random state parameter θ_i taken between $\frac{\theta_0}{2}$ and $\frac{3\theta_0}{2}$ is assigned to each stopping block. In this way, the heterogeneity of the basal properties can be reproduced and is sustained during the dynamic evolution of the system.

3.2. **Geometric parameters.** We first have to consider the geometric input parameters for modeling the Altelsgletscher. The glacier is discretized into a system of regular cubic blocks, whose weights remains constant during the numerical simulation. The application of this model to the time evolution of an unstable glacier

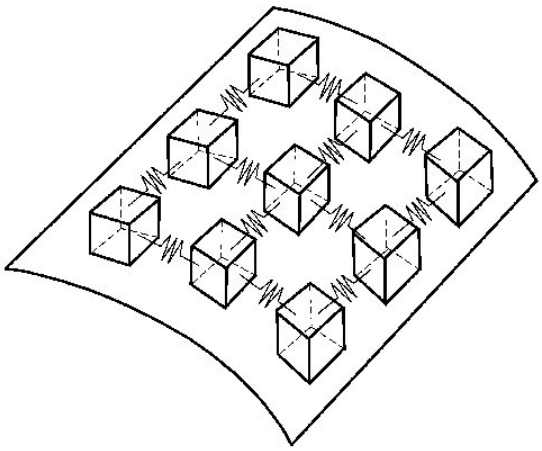

FIGURE 7. Illustration of the model constisting of spring-blocks resting on an inclined slope. The blocks lie on an inclined curved surface and gravity is the driving force. Only a small subset of the spring-block system is shown here.

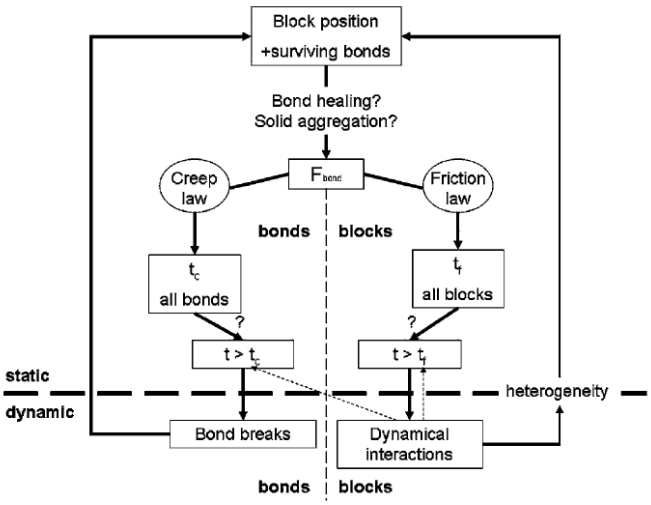

FIGURE 8. Schematic flowchart of this **modified spring-block** model.

implies that snow accumulation at the surface of the glacier is neglected, corresponding to a time scale of one-two years. This assumption seems to be justified for the Altelsgletscher as its northwestern face has a steep slope (from 35^o to 40^o) and is subjected to strong winds, drifting snow away. In addition, typical yearly

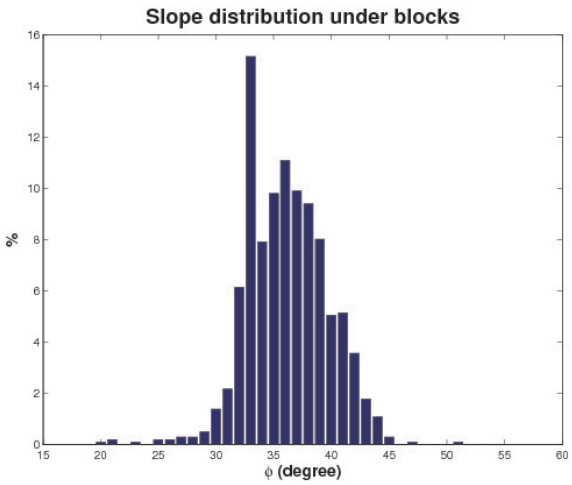

FIGURE 9. Distribution of the slope of the bedrock at position of the blocks.

additions of snow and ice are small compared with the overall thickness (around 30 meters) of the glacier.

In order to obtain a realistic description of the damage and fragmentation that may develop in the ice mass, we need a sufficiently large number of blocks. As a compromise between reasonable sampling and numerical speed, we use a model composed of 70×70 blocks for this particular example.

It is possible to evaluate the size of the unstable part from the analysis of Figure 2 and from direct observations. Accordingly, the glacier surface area was approximately 4 km^2, with a mean ice depth of 30 m. As we consider a model composed of 70×70 blocks, each block corresponds to a discrete mesh with 30 m thickness, 30 m length and 30 m width. The weight of each block is approximately equal to: 24.75×10^6 kg (with a density of 917 kg.m^{-3}).

The slope ϕ of the bedrock ranges from 35° (lower part) to 40° (upper part) (see Fig 9). To account for the curvature of the slope, we used a digital elevation model (see Fig. 10), supporting the blocks described above.

We now describe the two key processes in the model, the friction and damage laws, that are applied to blocks and bonds respectively.

3.3. **Friction law between the discrete blocks and the basal surface.** As a first guess of the input friction parameters of this model, we choose to start our investigations from the stablest case, i.e. cold ice, stuck onto the bedrock. Obviously, this was not the case, as explained in section 2.2. Nevertheless, it is a starting point for the parametrization of the initial friction properties.

We first make the assumption that the friction coefficient between the blocks and the underlying supporting sliding surface has constant properties. This is a simplification as the water pressure at the glacier bed typically oscillates with a daily periodicity (Iken, 1981; Bahr and Rundle, 1996). This assumption should however be valid in the case of a hanging glacier, for which, without change of

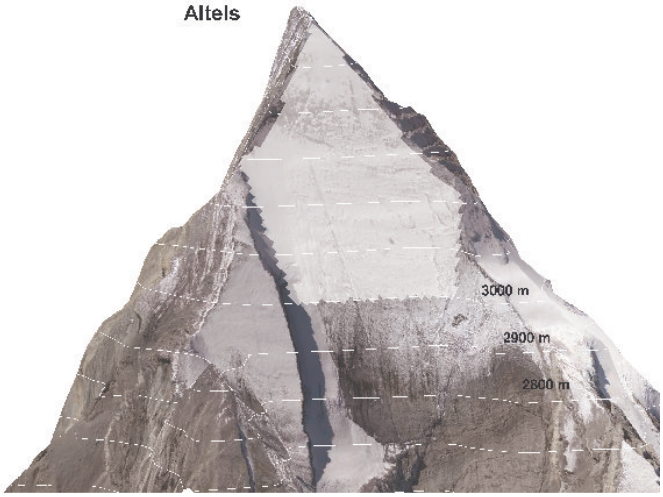

FIGURE 10. Digital elevation model of the Altels.

climatic conditions, the bedrock remains frozen and the ice remains cold during the whole year.

In the model, the friction between the discrete blocks and the basal properties is described with the following equation:

$$t_f \;=\; \frac{\theta_0}{\exp(\frac{\mu-\mu_0}{A}) - 1}\;, \tag{3.1}$$

where t_f is the time when the block starts sliding, μ_0 is a constant friction coefficient, A is a constant parameter depending on material property and θ_0 is the state parameter at steady state. μ is evaluated on each block with the definition of the solid friction $\mu = \frac{T}{N}$ where T are the tangential forces given by the position of its connected neighbors and N is the normal component of the weight of the block. Three parameters have to be evaluated to model the frictional processes within the glacier: μ_0, A and θ_0. In the stablest case, the rupture should nucleate and propagate within the ice. More generally, the glacier would not slide on its bedrock, but damage is concentrated in a sheared zone within the ice close to its base, resulting in an observable displacement at the glacier surface. Therefore, the friction law should represent the localization of shear within the ice, and the friction parameters should be taken to represent the physics of friction between ice surfaces.

Despite its importance, the topic of ice-ice friction has not yet been extensively studied, especially at low velocity. It is known that the ice-ice friction coefficient $\mu^{ice-ice}$ generally decreases with increasing sliding velocities and ambient temperature. It is also known that $\mu^{ice-ice}$ is relatively insensitive to both pressure and grain-size. Generally speaking, ice is regarded as a material which exhibits very low friction in sliding. However, at low sliding speed, the friction coefficient of ice can be considerably higher (Kennedy and others, 2000). These two different behaviors are generally explained by two physical mechanisms depending on the sliding velocity regimes:

(i) The first mechanism is the water lubrification mechanism (produced by frictional heat at the sliding surface) working at sliding velocity above roughly 0.01 m/s. The water lubrification mechanism is characterized by the low viscous resistance of water film produced by frictional heat at the sliding interface (Maeno and Arakawa, 2004; Barnes and others, 1971; Kennedy and others, 2000; Montagnat and Schulson, 2003).
(ii) The second mechanism is the adhesion and plastic deformation of ice at the friction interface, which is present at velocities lower than roughly 0.01 m/s (Kennedy and others, 2000; Montagnat and Schulson, 2003; Maeno and Arakawa, 2004).

Kennedy and others (2000) found the ice-ice friction coefficient to vary by about an order of magnitude (0.8 to 0.1) over a wide range of velocity (from 10^{-6} to 10^{-1} m/s). At low velocities ($< 10^{-5}$m/s), no systematic effect of temperature on friction was seen and tests performed at $-10°$C at velocities ranging from 10^{-6} to 10^{-1} m/s confirm that the nominal contact pressure has negligible effect on the friction coefficient (Kennedy and others, 2000). In a recent study, Maeno and Arakawa (2004) showed that the ice-ice friction coefficient becomes as high as 1.0 at 10^{-6}m/s for a temperature of ice of -10^{o}C, which is higher than values obtained by Kennedy and others (2000). They explained this large value by adhesion processes combined with ice sintering at the sliding interface.

As far as we are concerned, high friction should be considered for the Altels glacier for two main reasons:

(i) Its characteristic velocity is indeed very low, around 1 to 10 cm/day, thus far below 0.01 m/s.
(ii) The friction coefficient is independent of pressure. Thus, ice depth does not influence friction.

We thus choose a high value of the friction coefficient, namely the limit value $\mu_o^{ice-ice} \approx 1$ given by Maeno and Arakawa (2004).

Once the block slides, the dynamics is controlled by a kinetic friction coefficient, which is in general smaller than the static coefficient $\mu_o^{ice-ice}$. For low temperatures, Kennedy and others (2000) found a relatively constant value of the friction coefficient around 0.6 for sliding velocities below 10^{-4}m/s, and rapidly decreasing values at velocities above 10^{-4} m/s to 0.1. Because velocities above 10^{-4}m/s are not expected in our model describing the nucleation phase of the catastrophic rupture, we thus assume that the kinetic friction coefficient is $\mu_d = 0.6$.

Next, we turn to the coefficient A (and B since we have made the simplifying assumption that $B = A$) in the rate- and state-dependent friction law given by equation (3.2) Faillettaz and others (2010):

$$\mu(\dot{\delta}, \theta) = \mu_0 + A \ln \frac{\dot{\delta}}{\dot{\delta}_0} + B \ln \frac{\theta}{\theta_0} \ , \tag{3.2}$$

Here, $\dot{\delta}$ is the sliding velocity.

Laboratory experiments suggest that A is smaller than μ_0 by typically one and sometimes up to two orders of magnitude (Ohmura and Kawamura, 2007; Scholz, 2002, 1998). As we do not have access to strong experimental constraints, we choose $A \approx 0.1$, corresponding to one-tenth of the static friction coefficient.

The last parameter needed to parametrize the friction law is θ_0 defined by Faillettaz and others (2010)

$$\theta_0 = \frac{D_c}{\dot{\delta}_0}. \tag{3.3}$$

Here, $\dot{\delta}_0$ is generally interpreted as the initial low velocity of a sliding mass, before it starts to accelerate towards its dynamical instability. In the case of a glacier whose sliding velocity is typical small, i.e., of the order of centimeters per day, this suggests that a rough correct estimation is $\dot{\delta}_0 \approx 1$ cm.d^{-1}. D_c can be interpreted as a characteristic slip distance over which different asperities come in contact. It is difficult to evaluate this value. The recent seismological literature reports D_c to lie in the range of tens of centimeters to meters for earthquakes (Mikumo and others, 2003; Zhang and others, 2003). We arbitrary choose $D_c \simeq 1$ m. Finally, inserting this value in equation (3.3), we obtain $\theta_0 = 100$ days.

As explained in section 3.3, to account for the heterogeneity and roughness of the sliding surface, the state variable θ_i is reset to a new random value after the dynamical sliding stops. This random value should not be choosen too low in order to prevent a block which just stopped sliding from switching immediately in a new dynamical phase (i.e. $t_f = 0$). Thus, we assign $\theta_i = \nu.\theta_0$ with ν uniformly distributed between 0.5 and 1.5.

3.4. **Creep law.** As explained in section 3.1, bonds are modeled as linear springs in parallel with an Eyring dashpot. The springs transmit the forces associated with the relative displacements of the blocks. The spring stiffness has also to be evaluated in order to reflect the elastic property of the bulk ice mass. In continuous elasticity, Hooke's law of elasticity relates stress σ and strain ϵ via Young's modulus E: $\sigma = E\epsilon$. This leads to the expression: $\sigma_{bulk} = E_{ice}\frac{\delta L}{L}$. This stress is applied to a surface $S = L \times H$ (where H correspond to the height and L the length of the surface), leading to an equivalent force in the bulk equal to $F_{bulk} = E_{ice}\frac{\delta L}{L}\ S$. A linear spring is subjected to forces given by $F_{bond} = K_{bond}\ \delta L$. In order to find an equivalent behavior, these two forces have to be of the same order, leading to a spring stiffness given by $K_{bond} = E_{ice}H$. Usually, values for E_{ice} are reported to be 9 GPa (Petrovic, 2003; Petrenko and Whitworth, 1999). However, there is a disagreement of an order of magnitude between measurements of E in laboratory (9 GPa) and from field observation ($\approx$ 1GPa) as argued by Vaughan (1995).

Depending on the applied stress, ice has either a linear viscous behavior or a non-linear viscous behavior. In glaciers, ice creep is usually described by a non-linear viscous deformation called the Glen's flow law (see Hutter (1983) and references therein). This law relates, in steady-state conditions, strain rate and stress in the secondary creep regime. It is thus not possible with this law to describe the tertiary creep and the time rupture of a bond. Following Nechad and others (2005), non-linear viscous behavior is introduced in our model by the presence of the Eyring dashpot in parallel with a linear spring of stiffness E. Its deformation e is governed by the Eyring dashpot dynamics

$$\frac{de}{dt} = K \sinh(\beta s_{\text{dashpot}}) \tag{3.4}$$

where the stress in the dashpot is given by

$$s_{\text{dashpot}} = \frac{s}{1 - P(e)} - Ee\ , \tag{3.5}$$

Here, s is the total stress applied to the bond and $P(e)$ is the damage accumulated within the bond during its history leading to a cumulative deformation e. $P(e)$ can be equivalently interpreted as the fraction of representative elements within the bond which have broken, so that the applied stress s is supported by the fraction $1 - P(e)$ of unbroken elements. Following Nechad et al. [2005], we postulate the following dependence of the damage $P(e)$ on the deformation e:

$$P(e) = 1 - \left(\frac{e_{01}}{e + e_{02}} \right)^{\xi} , \tag{3.6}$$

where e_{01}, e_{02} and ξ are constitutive properties of the bond material.

Finally, by combining the previous equations, Faillettaz and others (2010) ended up with a creep model that computes the critical time (i.e. failure of the bond) as a function of the stress experienced by the bond s given by:

$$t_c = \begin{cases} \frac{1}{K} \exp(-\gamma\, s) & \text{if } s > s^\star \\ \to \infty & \text{if } s \leq s^\star \end{cases} \tag{3.7}$$

where

$$\gamma = \frac{\beta e_{02}^{\xi}}{e_{01}^{\xi}} \ . \tag{3.8}$$

and

$$s^\star = E \ \left(\frac{e_{01}}{\mu} \right)^{\mu} \ \left(\frac{\mu - 1}{e_{02}} \right)^{\mu - 1} . \tag{3.9}$$

Creep properties are defined by the parameters K, β, e_{01}, e_{02} and ξ, that we need to fix for our simulations.

We need to find the most appropriate parameters to describe creep behavior of ice. Natural glacier ice has a complex polycrystalline structure composed of crystals of different sizes. But ice is a fairly homogeneous material compared to fiber matrix composite. The more homogenous a material, the greater ξ. In the following, we set this value $\xi = 10$ (which means that ice is not very heterogeneous).

As Equation 3.6 shows, a fraction $1 - (e_{01}/e_{02})^{\xi}$ of all present representative elements undergo abrupt failure immediately after the stress is applied. Because ice does not show significant damage immediately after being loaded, this suggests to choose $e_{01} = e_{02}$, so that this fraction is vanishing.

The other parameters describing the deformation of the Eyring dashpot under an applied stress are β for the non-linear term and K for the linear one. For this study, we choose $\beta = 10^{-7}\,\mathrm{Pa}^{-1}$ and $K = 10^{-3}\,\mathrm{s}^{-1}$.

4. Numerical results

The aim of the numerical simulations is to test the different causes of the rupture, summarized in Röthlisberger (1981) and described in Section 2.2. In particular, we intend to provide answers to the following questions

- What is the influence of the glacier geometry on the dynamic of the instability?
- Can such a rupture happen without changes of the basal properties?
- How rapidly does the instability develop?
- Can we expect some precursors?

Geometric parameters					
n	m_{block}	ϕ			
-	kg	$^\circ$			
70	24.75×10^6	30 to 45			
Friction parameters					
A	θ_0	μ_0	$\dot{\delta_0}$		
-	d	-	$cm.d^{-1}$		
0.1	100	1	10^{-3}		
Creep parameters					
E	β	$C \sim 1/K$	ξ	e_{01}	e_{02}
Pa	Pa^{-1}	s	-	-	-
10^9	10^{-7}	10^3	10	0.003	0.003

TABLE 1. Parameters used for the simulation. n is the linear dimension of the lattice of blocks, which has a total of $n \times n$ blocks. The second row contains the list of parameters. The third row specifies the units of the parameters and in the fourth row the numerical values used in the simulation are given.

4.1. **Description of the simulation.** Blocks are distributed in a regular mesh along the slope, so that bonds are initially stress free. At each time step, we evaluate, on each block, the slope from the digital elevation model of the Altels area (see Fig. 10). This aims at mimicking the real topography of Altels glacier. To determine the causes of the glacier collapse, we will test the different contributions described by Röthlisberger (1981) (section 2.2).

The table 4.1 summarizes the parameters used in our simulations.

4.2. **Qualitative results.**

4.2.1. *Is the 1895 Altels collapse solely due to glacier thickening?* To answer this question, we tested the case of a constant friction coefficient in the presence of a progressive increase of the block weight. This means that mass is added at a constant rate on each block. In all the simulations performed, results show that an instability starts from the upper part of the glacier, in contradiction with observation (see Fig. 11). This could be explained by the bedrock topography: The slope is indeed steeper in the upper part, inducing an initial sliding of the upper blocks. Then, this instability propagates downwards and the whole glacier collapses.

The progressive thickening is therefore not the cause of the 1895 Altels break-off event.

4.2.2. *Is the 1895 Altels break-off due to uniform warming conditions at the bedrock?* At such altitude, the glacier is expected to be cold, i.e. stuck on its bedrock. But we saw that it experienced successive extreme hot summers, that could have initiated the phenomenon. Warming conditions could lead to a lubrication at the bedrock due to melted water penetration and consequent increase of basal water pressure. This can cause decoupling of the glacier with its bedrock and thus to decrease the friction between ice and bedrock. There are two ways to model uniform warming conditions in our model, first by decreasing uniformly the friction coefficient under each block, second by decreasing the tangential component of the weight of

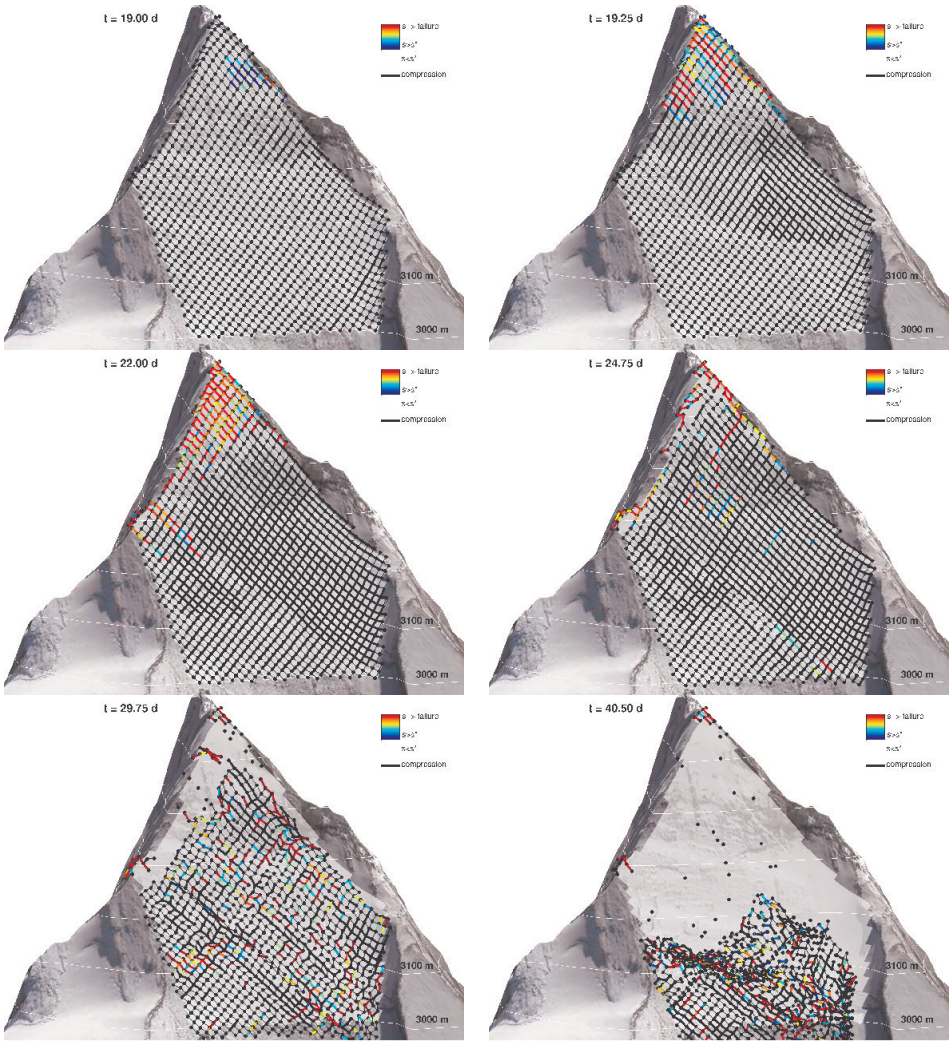

FIGURE 11. Six snapshots describing the rupture progression and sliding instability in the block lattice with constant friction coefficient μ_0 for all blocks in the presence of a progressive increase the block weights modeling snow/ice addition. The blocks are presented as points at the nodes of the square lattice. The color of each bond encodes the time remaining to rupture: red (close to rupture) to blue (far from rupture). Bonds in compression are drawn as thick black lines. Bonds without unstable tertiary creep damage are represented as thin black lines. Similar results are obtained by progressively decreasing the friction coefficient for all blocks.

each block. We tested both approaches which gave very similar qualitative results. Again, as expected, the whole glacier collapses, starting from its upper part (Fig. 11), for the same topographical reasons as explained above.

It also seems that differential evolution of the basal properties would affect the stability of this glacier.

4.2.3. *Is the 1895 Altels collapse due to a local increase of water pressure?* We now show that the **only way** to reproduce the geometry of the rupture is to progressively modify the basal properties in a restricted area, corresponding to the likely temperate area at the bedrock (Röthlisberger, 1981).

In the following, the friction coefficient is decreased with different rates $\frac{\delta\mu}{\delta t}$ on three different restricted areas (see Fig. 12) corresponding to the assumed temperate bedrock zone. In this way, we simulate the water penetrating within the glacier leading to a lubrification at the bedrock.

In the following, the value of μ_0 is set larger than $\arctan(\max(\phi))$, where ϕ is the slope evaluated from the Digital Elevation Model (DEM) of the glacier bed. In this way, the glacier is assumed to be stable when the simulation starts. At each numerical time step, the friction coefficient μ_0 is decreased by $\frac{\delta\mu}{\delta t}$.

4.2.4. *Qualitative description of the maturation of rupture in the case of a local evolution of basal properties:* Figure 13 shows the evolution of the set of blocks in the regime where an instability develops. Different phases can be distinguished during this simulation:

(i) Initially, blocks situated in the area where friction coefficient is decreased start sliding where the bedrock slope is largest. Sliding of these blocks lead to a change of stress experienced by the bonds. This internal bond deformation propagates upstream, as shown in Figure 13 (1)).

(ii) Then, the glacier starts accommodating its new stress state, resulting in a quiet phase. The number of sliding blocks progressively increases, leading to stronger interactions and to synchronization of the sliding blocks (see Figure 13, (4) and (5)).

(ii) After a certain time depending on $\frac{\delta\mu}{\delta t}$, the lattice starts fracturing. A large crack appears perpendicular to the main slope around the middle of the lattice (see Figure 13, (2) and (3)). This corresponds to the opening of the crevasse just below the bergschrund (Fig. 2).

(iv) A global instability develops. The blocks located below the upper crevasse start to accelerate and a fracture propagates in the bedrock slope direction, forming an unstable slab which finally slides off (see Figure 13, (6)).

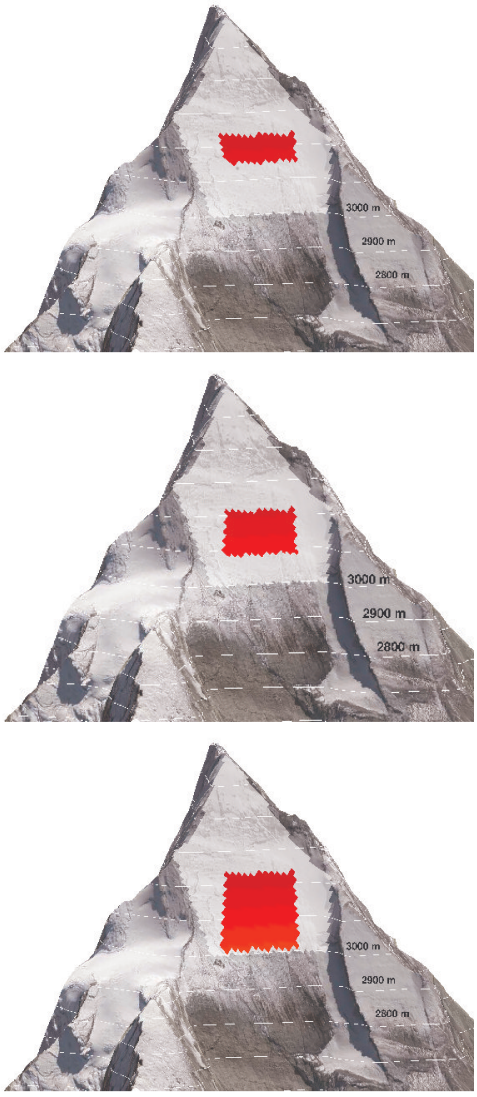

FIGURE 12. Zones where the basal friction coefficient is decreased. Their geometrical limits were determined according to Röthlisberger (1981), see Fig. 5.

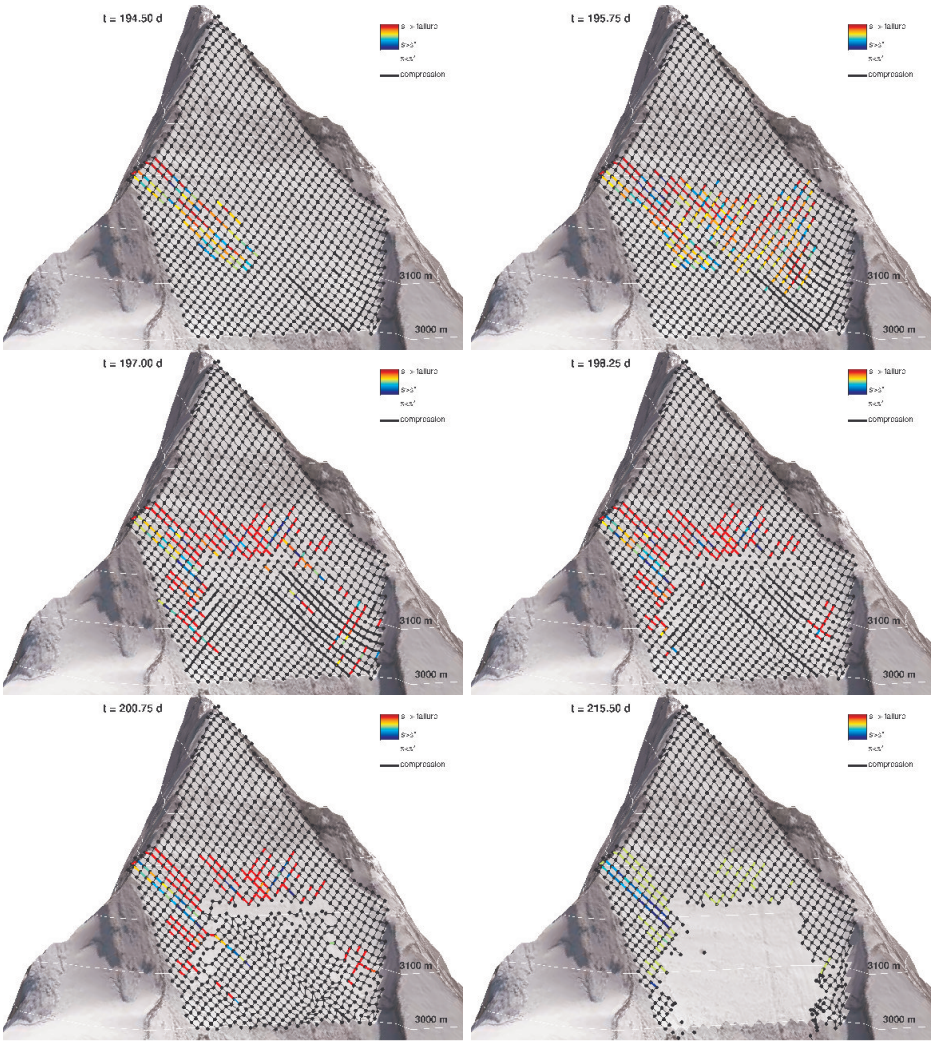

FIGURE 13. Six snapshots describing the rupture progression and sliding instability in the block lattice for the largest zone where basal friction coefficient was progressively reduced. The blocks are presented as points at the nodes of the square lattice. The color of each bond encodes the time remaining to rupture: red (close to rupture) to blue (far from rupture). Bonds in compression are drawn as thick black lines. Bonds without unstable tertiary creep damage are represented as thin black lines.

4.3. **Quantitative results.** The results obtained with the spring-block model can be summarized as follows.

4.3.1. *Initiation of the instability.* For each of the three process zones (i.e. the area where the friction coefficient is decreased) and for different rates $\delta(\mu)/\delta(t)$ of decrease of the coefficient of friction (RDCF), we have plotted the number of sliding blocks at each time step (see Fig. 14). It appears that, in all cases, the initiation of the instability occurs very suddenly, typically within one or two days. Two different regimes could also be distinguished. A first quiescent one, where isolated blocks slide, and a second active one, where blocks start to slide in clusters leading to the final collapse.

The number of sliding blocks after the onset of the instability depends on the RDFC. The greater the RDCF, the larger the number of sliding block. When the RDCF is small, the glacier has time to adapt to the changes of basal conditions. In this case, the size of the initial unstable cluster is strictly given by the size of the process zone.

4.3.2. *Damage evolution within the glacier.* In order to measure the damage evolution within the glacier, we count the number of surviving bonds during each simulation. Fig. 15 shows the number of surviving bonds within the lattice at each time step, for different process zones and different rates of decrease of the friction coefficient (RDCF). A rapid increase of the damage a few days after the initiation of the instability can be observed for all simulations. Moreover, this increase does not seem to depend on the rate of decrease of the friction coefficient. Results show that, once the behavior enters in the active regime, bonds start to fail, leading to the openning of the crown crevasse. This crevasse opens very rapidly, typically in a few days, which was also observed (Heim, 1895).

4.3.3. *Energy analysis.* In order to detect precursors to the rupture, we plotted the evolution of the energy stored in the bonds, the kinetic energy and the radiated energy during the destabilization process.

A typical result is shown in Fig. 16. Six phases can be distinguished. (1) The glacier is still in a stable phase. (2) Initiation of the instability. (3) The number of sliding blocks drastically increases. (4) The number of sliding blocks reaches a maximum and the energy stored in the bonds increases. Note that the increase of kinetic and radiated energies starts to be visible. (5) The energy stored in the bonds drops because the crown crevasse opens up. The number of sliding blocks remains unchanged and the instability is now established. Both the kinetic and radiated energies increase. (6) After an increase of the energy stored in the bonds, cluster of bonds are failing.

These results show that no precursor of the instability can be inferred from the time evolution of the different types of energy more than a few days before the break-off.

4.3.4. *Occurrence of the instability as a function of $\delta(\mu)/\delta(t)$.* To assess if the rate of decrease of the friction coefficient (RDFC: $\delta(\mu)/\delta(t)$) influences the final time of rupture, we performed independent runs with different rates and evaluated their respective rupture times. The results show that the rupture occurs earlier for greater RDFC, which is not surprising (see Fig. 17). However, the time of rupture does not depend linearly on RDFC but follows a power-law with an exponent of

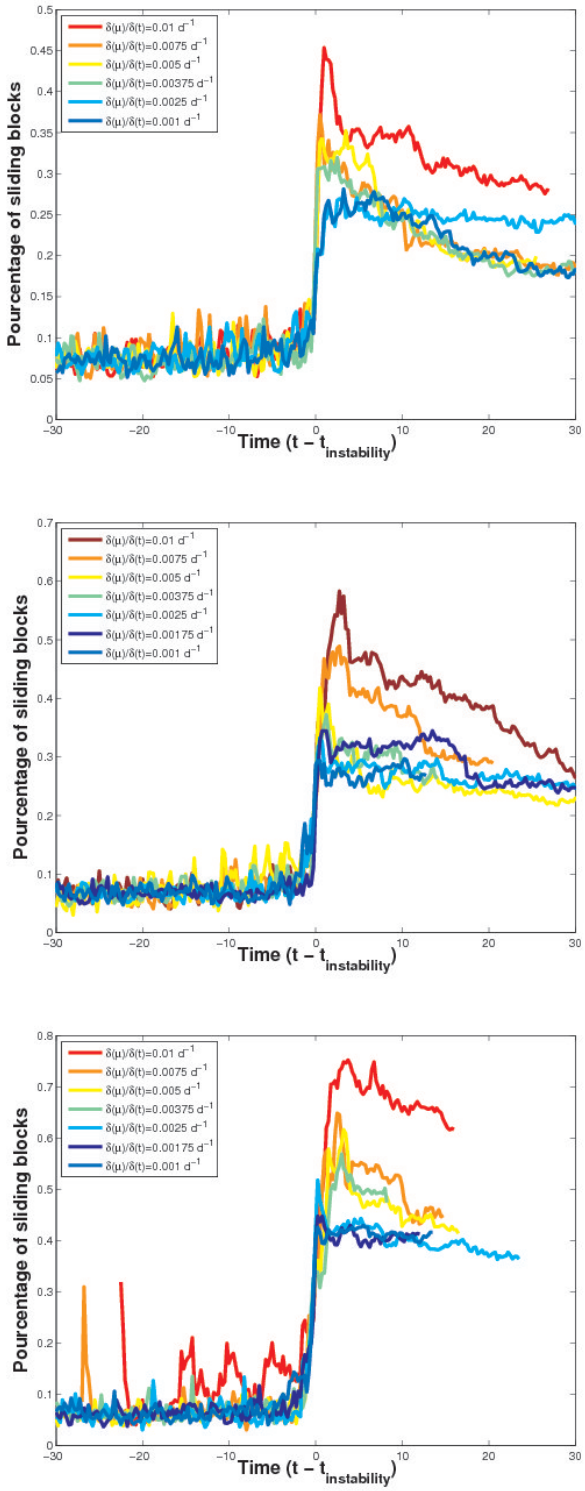

FIGURE 14. Percentage of sliding blocks within the glacier for different $\frac{\delta\mu}{\delta t}$ as a function of time, for the three different process zones (resp. minimum, medium and maximum corresponding to the top to bottom panels of fig. 12).

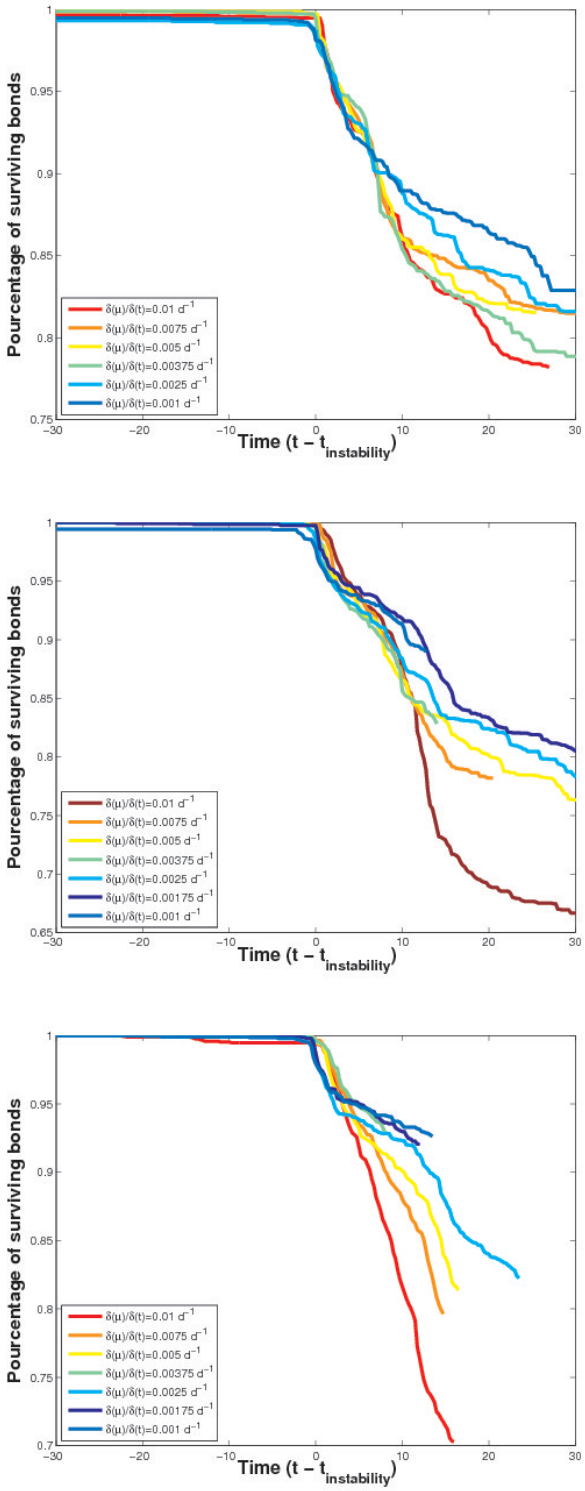

FIGURE 15. Percentage of the surviving bonds within the glacier for different rate $\frac{\delta\mu}{\delta t}$ of decrease of the coefficient of friction (RDCF) as a function of time, for the three different process zones (resp. minimum, medium and maximum corresponding to the top to bottom panels of fig. 12).

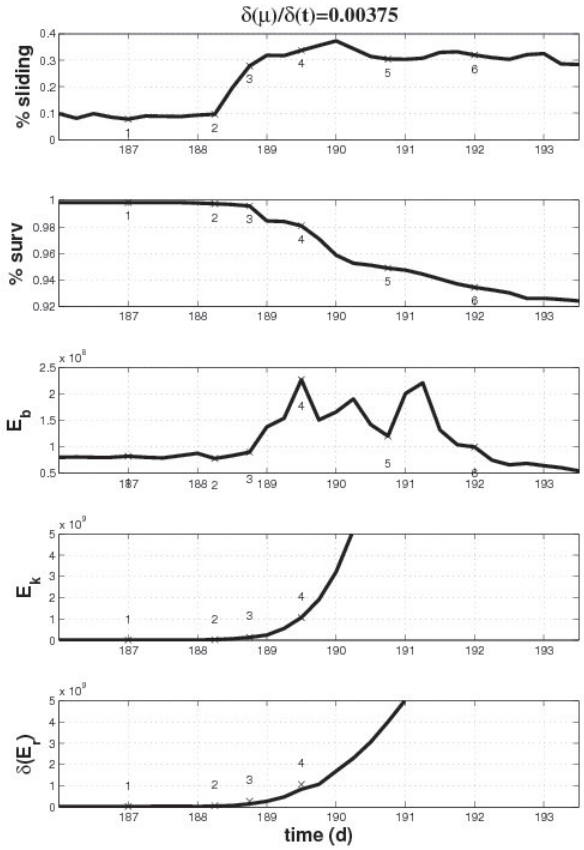

FIGURE 16. Evolution of the energy stored in the bonds, of the kinetic energy and of the radiated energy during the destabilization process.

-0.82. This means that, for small RDFC, the glacier has time to adapt to these changes and the final instability arises later than in the case of large RDFC.

The influence of the area of the process zone was tested and we found an inverse effect compared with the RDFC. Specifically, a glacier for which a large RDFC acts on a small process zone becomes unstable after the same time as a glacier subjected to a small RDFC applied to a large process zone. This can be summarized by plotting the reduced variable $t_c * A^{0.78}$ as a function of $(\frac{\delta(\mu)}{\delta(t)})^{-0.82}$, as shown in Fig. 18.

Unfortunately, in a real situation, the a priori determination of these parameters (RDFC and process zone area) is far from being possible, especially for the area of the process zone.

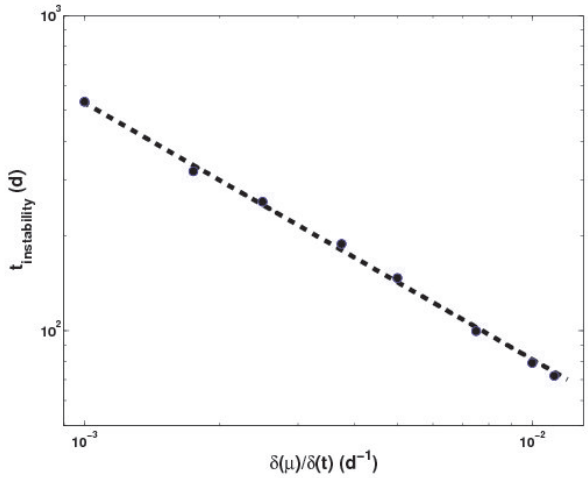

FIGURE 17. Time of rupture as a function of the RDCF $\delta(\mu)/\delta(t)$, for the medium process zone. The dotted line plots the equation: $t_i \sim (\frac{\delta(\mu)}{\delta(t)})^{-0.82}$

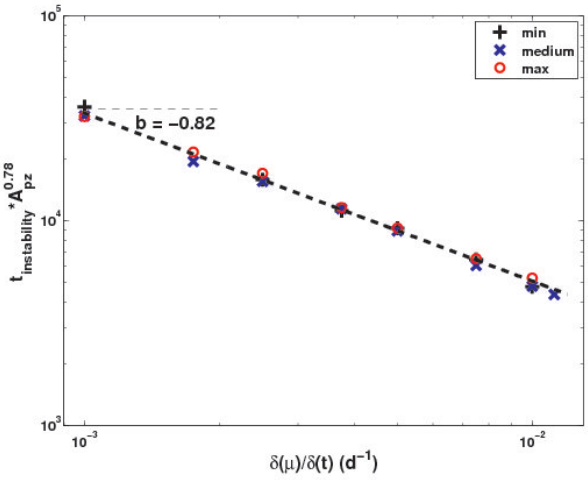

FIGURE 18. Time of rupture as a function of $\delta(\mu)/\delta(t)$. The dotted line plots the equation: $t_i \cdot A^{0.78} \sim 116 \cdot (\frac{\delta(\mu)}{\delta(t)})^{-0.82}$

5. CONCLUSION

The Altels glacier fall of 1895 is the largest ice fall known in the Alps. The mechanisms leading to this event are not fully understood. With a new model developed by Faillettaz and others (2010) of the progressive maturation of a heterogenous mass towards a gravity-driven instability, characterized by the competition between frictional sliding and tension cracking, we have contributed to a better understanding

of this event. We used an array of sliding blocks on an inclined (and curved) basal topography, which interacts via elastic-brittle springs. A realistic state- and rate-dependent friction law was used for the block-bed interaction. We modeled the inner material properties of the mass and its progressive damage eventually leading to failure, by means of a laboratory-based stress corrosion law governing the rupture of the springs.

Our simulations showed that the only way to reproduce the particular arch shape of the crown crack of the Altels glacier fall was to reduce the basal friction coefficient in a limited area. Such a break-off arises because of the onset of a weak zone at the interface between the glacier and its bedrock, probably due to melted water infiltrations trapped within the glacier. Climatic observations before the collapse support this assumption as they showed hot summers before the instability, explaining such melted water infiltrations.

Moreover, a two-step behavior could be evidenced in our simulations: (i) a first quiescent phase, without visible changes with a duration depending on the rate of decrease of the friction coefficient (RDFC). (ii) An active regime with a rapid increase of basal motion within a few days before the break-off. As a consequence, a crown crevasse opens a few days later (which was observed) and the final rupture occurs. This means that the destabilization process of a hanging glacier due to a progressive warming of the ice/bed interface towards a temperate regime is expected to occur without visible signs until a few days prior to the collapse.

The area of the process zone and the RDFC have an equivalent relative influence on the time of the onset on the instability. A small area of process zone with a large RDFC would lead to the same behavior as a large area of process zone with a small RDFC. From a practical point of view, the knowledge of both parameters is needed to predict the onset of such an instability. The determination of these two parameters is not yet possible, especially for the area of the process zone. The collapse of three power laws shown in Fig. 18 can be rewritten as $t_i \sim (A \cdot (\delta\mu/\delta t))^{-\nu}$, where $\nu \approx 0.8$. This law expresses a combined "size" effect (through the term A) and a rate-dependence effect (through the term $\delta\mu/\delta t$), which is also found qualitatively similar in most heterogenous mechanical systems going to failure (Carpinteri, 1995; Collins, 1993). Interestingly, the combined dependence of the failure time t_i on the unstable area A and on the rate $\delta\mu/\delta t$ is through their product, suggesting that the driving mechanism for the failure time is the total shear force applied to the unstable area.

A recent paper Faillettaz and others (2011) showed that seismic measurements could help predict the approaching mechanical instabilities of cold hanging glaciers with the help of some seismic precursors (e.g. by using changes in the statistical behavior of icequakes), before the instability becomes obvious by its visual impacts. Unfortunately, we could not find any seismic precursors for instabilities driven by infiltrated melted water.

In a more general context, global climate warming may influence the stability of cold hanging glaciers. Moreover, as the rupture process takes some time to develop and external precursors are only visible a few days prior to the break-off, some cold hanging glaciers could already be in the unstable phase where the instability is already developing. An early warning of such events is still far from beeing possible.

References

Abele, G. 1974. Bergstürze in den Alpen. Ihre Verbreitung, Morphologie und Folgeerscheinungen. Wissensch. Alpenverreinshefte, 25, München.

Andersen, J.V., D. Sornette and K.-T. Leung. 1997. Tri-critical behavior in rupture induced by disorder, *Phys. Rev. Lett.*, **78**, 2140-2143.

Bahr, D.B. and J.B Rundle. 1996. Stick-slip statistical mechanics at the bed of a glacier. *Geophys. Res. Lett*, **23**, (16), 2073-2076.

Barnes, P., D. Tabor, F. R. S. Walker and J. C. F. Walker. 1971. The friction and creep of polycrystalline ice. *Proc. Roy. Soc. Lond. A.*, **324**, 127-155.

Begert, M., T. Schlegel, and W. Kirchhofer. 2005. Homogeneous temperature and precipitation series of Switzerland from 1864 to 2000, *Int. J. Climatol.*, **25**(1), 65-80, doi:10.1002/joc.1118.

Carpinteri, A. 1995. Size-Scale Effects in the Failure Mechanisms of Materials and Structures, Taylor and Francis, 1995 - Technology & Engineering

Collins, J.A. 1993. Failure of materials in mechanical design (Analysis, prediction, prevention), 2nd ed., John Wiley & sons, New York (1993)

Du Pasquier, L. 1896. L'avalanche du glacier de l'Altels le 11 septembre 1895. *Annales de Géographie*, **5**, (23), 458-468.

Faillettaz, J., A. Pralong, M. Funk and N. Deichmann. 2008. Evidence of log-periodic oscillations and increasing icequake activity during the breaking-off of large ice masses. *J. Glaciol.*, **57**, (187), 725.

Faillettaz, J., D. Sornette, and M. Funk. 2010. Gravity-driven instabilities: interplay between state-and-velocity dependent frictional sliding and stress corrosion damage cracking. *J. Geophys. Res.*, **115**, B03409, doi:10.1029/2009JB006512. arXiv/0904.0944.

Faillettaz, J., D. Sornette and M. Funk. 2011. Icequakes coupled with surface displacements for predicting glacier break-off. *accepted to J. Glaciol.* arXiv:1011.4781v1

Flotron, A. 1977. Movement studies on hanging glaciers in relation with an ice avalanche, *J. Glaciol.*, **19** (81), 671–672.

Forel, F. A. 1895. L'éboulement du glacier de l'Altels. *Archive des sciences physiques et naturelles*, Genève, t.**34**, 513-543.

Heim, A. 1895. Die Gletscherlawine an der Altels am 11. September 1895. Zürcher aund Fürrer, Zürich.

Heim, A. 1932. Bergsturz und Menschenleben, Fretz und Wasmuth, Zürich.

Hock, R. 2003. Temperature index melt modeling in mountain regions. *J. Hydrol.*, **282**(1-4), 104-115. doi:10.1016/S0022-1694(03)00257-9.

Hutter, K. 1983. Theoretical glaciology; material science of ice and the mechanics of glaciers and ice sheets. D. Reidel Publishing Company/Tokyo, Terra Scientific Publishing Company.

Iken, A. 1981. The effect of the subglacial water pressure on the sliding velocity of a glacier in an idealized numerical model. *J. Glaciol.*, **27**, (97), 407-421.

Kennedy, F.E., E.M. Schulson and D.E. Jones. 2000. The friction of ice at low sliding velocities, *Philos. Mag. A*, **80** (5) 1093-1110.

Leung, K. and J.V. Andersen. 1997. Phase transition in a spring-block model of surface fracture, *Europhys. Lett.*, **38** (8), 589-594.

Lüthi, M. 2003. Instability in glacial systems, Milestones in Physical Glaciology: From the Pioneers to a Modern Science, **180**, 63–70, VAW, ETH-Zürich.

Maeno, N. and M. Arakawa. 2004. Adhesion shear theory of ice friction at low sliding velocities, combined with ice sintering. *J. Appl. Phys.*, **95**(1), 134-139.

Mikumo, T., K. B. Olsen, E. Fukuyama and Y. Yagi. 2003. Stress-breakdown time and slip-weakening distance inferred from slip-velocity functions on earthquake faults, *Bull. Seism. Soc. Am.*, **93**, 264-282.

Montagnat, M. and E. Schulson. 2003. On friction and surface cracking during sliding of ice on ice. *J. Glaciol.*, **49** (166), 391-396.

Nechad, H., A. Helmstetter, R. El Guerjouma and D. Sornette. 2005. Creep Ruptures in Heterogeneous Materials, *Phys. Rev. Lett.*, **94**, 045501.

Ohmura, A. and H. Kawamura. 2007. Rate- and state-dependent friction law and statistical properties of earthquakes. *Europhys. Lett.*, **77**(6), 69001 (5pp).

Petrovic, J.J. 2003. Mechanical properties of ice and snow. *J. Mater. Sci.*, 38, 1-6.

Petrenko,V.F. and R.W. Whitworth. 1999. Physics of ice. Oxford University Press, 384pp.

Pralong, A. and M. Funk .2005. Dynamic Damage Model of Crevasse Opening and Application to Glacier Calving, *J. Geophys. Res.*, **110**: B01309.

Pralong, A. and M. Funk. 2006. On the instability of avalanching glaciers, *J. Glaciol.*, **52** (176): 31–48.

Pralong, A., C. Birrer, W. Stahel and M. Funk. 2005. On the Predictability of Ice Avalanches, *Nonlinear Processes Geophys*, **12**, 849–861.

Raymond, M., M. Wegmann and M. Funk. 2003. Inventar gefährlicher Gletscher in der Schweiz, *Mitteilung*, **182**, VAW, ETH Zürich.

Röthlisberger, H. 1981. Eislawinen und Ausbrüche von Gletscherseen, in P. Kasser (Ed.), Gletscher und Klima - glaciers et climat, Jahrbuch der Schweizerischen Naturforschenden Gesellschaft, wissenschaftlicher Teil 1978,pp 170–212, Birkhäuser Verlag Basel, Boston, Stuttgart.

Scholz, C.H. 1998. Earthquakes and friction laws, *Nature*, **391**, 37-42.

Scholz, C.H. 2002. The mechanics of earthquakes and faulting (Cambridge University Press).

Vaughan, D. 1995. Tidal flexure at ice shelf margins. *J. Geophys. Res.*, **100** (B4), 6213-6224.

Zhang, W., T. Iwata, K. Irikura, H. Sekiguchi and M. Bouchon. 2003. Heterogeneous distribution of the dynamic source parameters of the 1999 Chi-Chi, Taiwan, earthquake, *J. Geophys. Res.*, **108** (B5), 2232, doi:10.1029/2002JB001889.

J. Faillettaz, VAW, ETH Zurich, Laboratory of Hydraulics, Hydrology and Glaciology, Switzerland
E-mail address: faillettaz@vaw.baug.ethz.ch

DD. Sornette, epartment of Management, Technology and Economics, ETH Zürich

Department of Earth Sciences, ETH Zürich

Institute of Geophysics and Planetary Physics, UCLA
Current address: Department of Management, Technology and Economics,, ETH Zürich, Switzerland
E-mail address: dsornette@ethz.ch

M. Funk, VAW, ETH Zurich, Laboratory of Hydraulics, Hydrology and Glaciology, Switzerland
E-mail address: funk@vaw.baug.ethz.ch